Available online at www.sciencedirect.com
ScienceDirect
Journal of Solid State Chemistry 180 (2007) 1538–1546
JOURNAL OF SOLID STATE CHEMISTRY
www.elsevier.com/locate/jssc

The crystallographic and magnetic characteristics of Sr_2CrO_4 (K_2NiF_4-type) and $Sr_{10}(CrO_4)_6F_2$ (apatite-type)

Tom Baikie[a,*], Zahara Ahmad[a], Madhavi Srinivasan[a], Antoine Maignan[b], Stevin S. Pramana[a], T.J. White[a]

[a]*Division of Materials Science, Nanyang Technological University, 50 Nanyang Avenue, 639798 Singapore, Singapore*
[b]*Laboratoire CRISMAT, UMR CNRS 6508, ISMRA-ENSICAEN, 6 Boulevard du Maréchal Juin, 14050, Caen, Cedex, France*

Received 27 November 2006; received in revised form 15 February 2007; accepted 25 February 2007
Available online 7 March 2007

Abstract

Solid-state reaction between $SrCO_3$, Cr_2O_3 and SrF_2 has produced the apatite phase $Sr_{10}(CrO_4)_6F_2$ and Sr_2CrO_4 which adopts the K_2NiF_4-type structure. The reaction outcome was very sensitive to the heating rate with rapid rise times favouring the formation of Sr_2CrO_4, which has been synthesised at ambient pressure for the first time. Powder X-ray diffraction and electron diffraction confirmed that Sr_2CrO_4 adopts a body centred tetragonal cell (space group $I4/mmm$) with lattice parameters $a = 3.8357(1)$ Å and $c = 12.7169(1)$ Å, while a combination of neutron and X-ray diffraction verified $Sr_{10}(CrO_4)_6F_2$ is hexagonal (space group $P6_3/m$) with lattice parameters $a = 9.9570(1)$ Å and $c = 7.4292(1)$ Å. X-ray photoelectron spectroscopy and magnetic measurements were used to characterise the oxidation states of chromium contained within these phases.

Keywords: Apatite; Ruddlesden–Popper; Chromate; Powder X-ray/neutron diffraction; Electron diffraction; XPS

1. Introduction

The influence of the discovery of high T_c superconductors (HTSC) [1] on contemporary inorganic solid-state chemistry has been enormous [2]. One consequence has been that the chemistry of inorganic solids containing transition metals, long a pillar of condensed matter research, was partially deprived of its intrinsic diversity and restricted almost entirely to the search for cuprates showing superconducting properties [3]. On the other hand, the complexity of the phenomenon of HTSC required an understanding of one- or two-dimensional magnetic interactions between unpaired spins of Cu^{2+} cations and this generated interest in low-dimensional magnetism. The realisation that a deeper understanding of these interactions would elucidate the incompletely understood mechanism of superconductivity has encouraged the investigation of materials other than cuprates, which in turn is leading to a more balanced appreciation of the chemistry of the transition metal oxides.

The perovskite family or more generally their Ruddlesden–Popper (RP) [4] derivatives with general formula $A_{n+1}B_nX_{3n+1}$ (where A is usually an alkaline earth or lanthanide cation, B is usually a transition metal and X is usually oxygen) is the most common structural family to display HTSC behaviour. The search for RP-type phases containing transition metals other than copper has revealed giant and colossal magnetoresistive effects in RP-type cobaltites [5] and manganites [6], respectively. More generally, RP chemistry is diverse, although RP-type phases containing chromium are less common and difficult to prepare under conventional synthetic conditions. For example, it has been reported that Sr_2CrO_4 synthesised under solid-state reaction conditions in air does not adopt a K_2NiF_4-type [7] structure (see Fig. 1) but is a β-K_2SO_4-type with the Cr^{4+} ions in isolated tetrahedral coordination [8,9]. Kafalas et al. [10] synthesised K_2NiF_4-type Sr_2CrO_4 via a high-pressure reaction between Sr_2CrO_4 (β-K_2SO_4-type) and CrO_2 at 65 kbar and 1000 °C. Matsuno

*Corresponding author. Fax: +65 6790 9081.
E-mail address: tbaikie@ntu.edu.sg (T. Baikie).

0022-4596/$ - see front matter © 2007 Elsevier Inc. All rights reserved.
doi:10.1016/j.jssc.2007.02.023

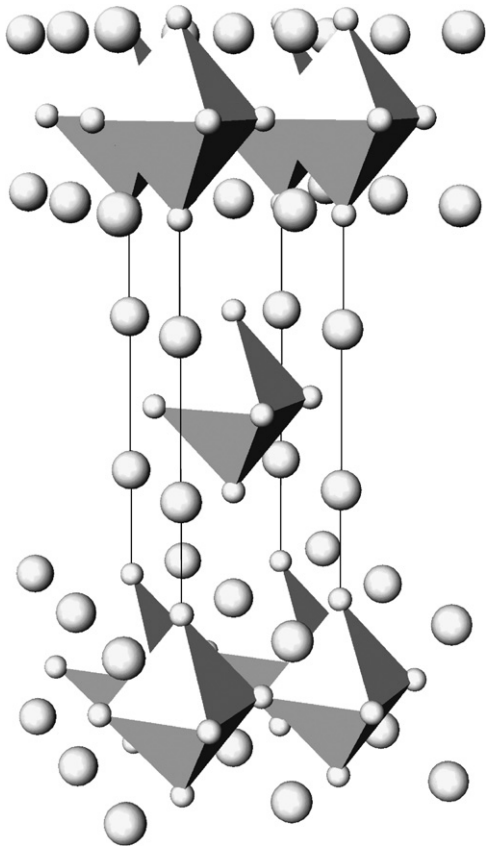

Fig. 1. A structural representation of Sr_2CrO_4 with the larger spheres representing Sr and polyhedra representing CrO_6 octahedra with the O ions shown as smaller spheres. Unit-cell indicated by black lines.

et al. also prepared a thin film sample of a K_2NiF_4-like Sr_2CrO_4 phase using pulsed-laser deposition (PLD) but were unable to prepare a bulk sample [11]. This work identified an orthorhombic unit cell that was determined from its optical conductivity spectra to have an insulating ground state. This is in strong contrast to the cubic perovskite $SrCrO_3$ that is reported to be metallic [12,13]. In addition, Pelloquin et al. [14] prepared the K_2NiF_4-related phase $Sr_{4.5}Cr_{2.5}O_9$ that was shown by high resolution transmission electron microscopy (HRTEM) to adopt a super-structure consisting of ordered intergrowths of $[Sr_2CrO_4]$ and $[(Sr_{0.5}Cr_{0.5})Sr_2CrO_5]$ blocks. This structure contained mixed chromium coordination and valence, forming $Cr^{6+}O_4$ tetrahedra, $Cr^{3+}O_6$ octahedra and $Cr^{3+}O_5$ square pyramids analogous to the superconducting cuprate $TlBa_{2-x}La_{2+x}Cu_2O_9$ [15].

This article describes the synthesis of a K_2NiF_4-type Sr_2CrO_4 phase at ambient pressure without the appearance of a super-structure. In the course of this study, the apatite phase $Sr_{10}(CrO_4)_6F_2$ was also produced. While this phase has been reported previously [16–18], only lattice parameters were given and no XPS or magnetic studies carried out. Therefore, Rietveld refinement of this phase combining the techniques of powder X-ray and neutron diffraction was undertaken and the magnetic properties investigated for the first time. These observations are of fundamental interest, as the appearance of Cr^{5+} is rare but has been identified in apatite ($A_{10}(CrO_4)_6X_2$) and the related mineral phase spodiosite $A_2(CrO_4)_2X$ (A = Ca, Sr and Ba) X = OH, Cl and F) [17].

2. Experimental methods

The preparation of Sr_2CrO_4 and $Sr_{10}(CrO_4)_6F_2$ was achieved via a solid-state reaction between $SrCO_3$, Cr_2O_3 and SrF_2 mixed in various molar ratios and treated at temperatures ranging 800–1000 °C for 10–40 h under a nitrogen atmosphere. The reaction products were characterised using a combination of powder X-ray (PXRD) and neutron diffraction (PND) and selected area electron diffraction (SAED). The PXRD patterns were collected using a Shimatzu diffractometer (Cu-Kα radiation) over the angular range 10–140° 2θ with a step size of 0.02° and a dwell time of 10 seconds per step. The patterns were analysed by the Rietveld method [19] using the fundamental parameters approach [20] contained within the software TOPAS V3 (Bruker-AXS). Powder neutron diffraction data were collected on the high resolution powder diffractometer (HRPD) at the High Flux Australian Reactor (HIFAR) operated by the Australian Nuclear Science and Technology Organisation (ANSTO). A neutron wavelength of 1.8845 Å was used from 0.029° to 150.079° 2θ in 0.05° steps. Approximately, 15 g of the apatite was loaded into a 12 mm diameter vanadium can that was rotated during data collection. Rietveld refinements employed a pseudo-Voigt peak shape corrected for asymmetry and the scattering lengths 0.7020, 0.3635, 0.5803 and 0.5654×10^{-12} cm were used for Sr, Cr, O and F, respectively.

Powder specimens for examination by transmission electron microscopy (TEM) were ground under ethanol, dispersed in an ultrasonic bath for several minutes and a drop of the suspension deposited onto a holey-carbon coated copper-grid. SAED patterns were collected using a JEOL-2100 microscope operated at 200 kV. A Gatan double tilt holder was employed to tilt crystals to the principle crystallographic orientations.

The oxidation states of chromium in Sr_2CrO_4 and $Sr_{10}(CrO_4)_6F_2$ were analysed using a PHI 5600 X-ray photoelectron spectrometer (XPS). Sample powders were dusted onto a polymeric based adhesive tape on an aluminium sample stub. All spectra were recorded using a Mg Kα_1 X-ray radiation source (1253 eV) with a scan range of 0–1000 eV binding energy (BE). The analysis chamber pressure was 8.0×10^{-9} torr. High resolution spectra for chromium were recorded in the selected energy range of 569–593 eV. Peak deconvolution, fitting and data analysis were carried out using CASA (computer aided surface analysis) XPS software (ver 2.3.10). BE values were referenced against adventitious carbon (C 1s = 284.8 eV). The Cr $2p_{3/2}$ and Cr $2p_{1/2}$ lines were fitted using a Voigt function with 30% Lorentzian character and included a Shirley background. The components of the Cr-peaks were

constrained by setting the Cr $2p_{3/2}$/Cr $2p_{1/2}$ ratio for each set of the spin–orbit doublets to the theoretical ratio of 4:2 [21] and the full width half maximum (FWHM) ratio was assumed to be unity [22].

Magnetic susceptibility measurements were conducted in a quantum design superconducting quantum interference device (SQUID magnetometer) over the temperature range 4–350 K with a magnetic field of 3000 Oe.

3. Results and discussion

3.1. Structural properties

3.1.1. Sr_2CrO_4

The PXRD pattern of the product from reaction between $SrCO_3$, Cr_2O_3 and SrF_2 in the ratio 9:3:1 performed under a nitrogen atmosphere at 1000 °C, using a heating rate of 300 °C h^{-1}, a dwell time of 20 h and furnace cooling the sample to room temperature indicated the formation of an $n = 1$ RP-type phase (K_2NiF_4-type) of Sr_2CrO_4. The sample was not single phase and a small number of the unknown reflections were possibly attributable to 'CrO_2F_2'; however, this phase remains partially characterised with only *d*-spacings having been reported [23]. As the reported *d*-spacings for 'CrO_2F_2' did not account for all of the unknown reflections the presence of other unknown phases cannot be excluded.

The powder pattern was refined using a structural model based on an $n = 1$ RP-type structure with regions containing the unknown reflections excluded from the refinement (Fig. 2). As the software TOPAS does not include the atomic scattering factor for Cr^{4+} this atomic site was refined with the form factor for the isoelectronic ion V^{3+}. All atomic sites refined to within one standard deviation of the expected full site occupancy, however the thermal parameter for the Cr is quite large (1.47 $Å^2$). The crystallographic data of Sr_2CrO_4 are given in Tables 1 and 2 with the refinement proceeding smoothly to an $R_{Bragg} = 4.9\%$. The Cr–O bond lengths show that the CrO_6 octahedra are distorted with the axial Cr–O distances (2.070(9) Å) significantly longer than the equatorial (1.918(9) Å). The lattice parameters while comparable to those obtained

Table 2
Selected bond lengths for Sr_2CrO_4 (ax = axial, eq = equatorial)

Bond	Sr_2CrO_4 (Å)
Sr–Sr	> 3.596(7)
Sr–Cr	3.254(4)
Sr–O(1)	2.629(5)
Sr–O(2)(ax)	2.494(9)
Sr–O(2)(eq)	2.726(1)
Cr–O(1) (eq)	1.918(9)
Cr–O(2) (ax)	2.070(9)

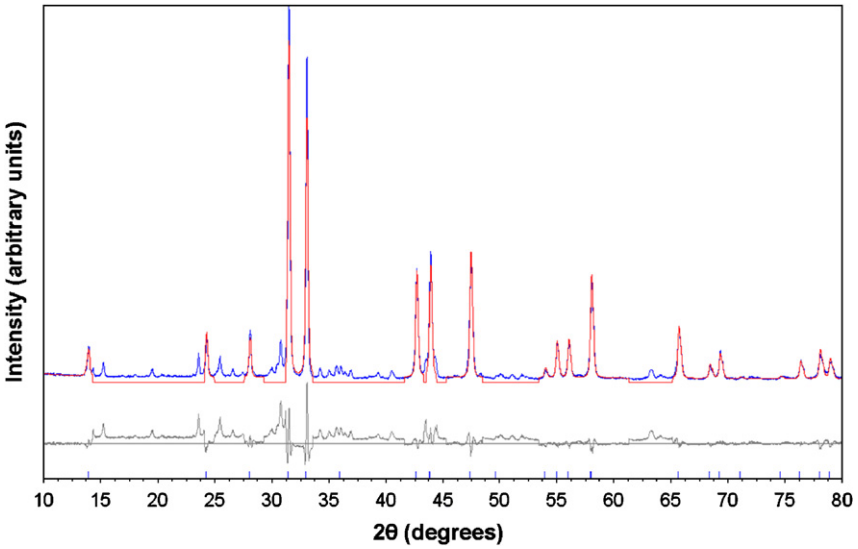

Fig. 2. Rietveld analysis of the PXRD pattern of Sr_2CrO_4. The regions where the background is lower were excluded from the refinement.

Table 1
Refined atomic positions for Sr_2CrO_4

S.G.	*I4/mmm*	$a = 3.8357(1)$ Å	$c = 12.7169(1)$ Å	$R_{wp} = 14.2\%$	$R_{Bragg} = 4.9\%$	Occ.
	Wyckoff	*x*	*y*	*z*	B_{eq}	
Sr	4e	0	0	0.3589(2)	1.27(2)	1.0(1)
Cr	2a	0	0	0	1.47(5)	1.0(1)
O(1)	4c	0	0.5	0	1.10(13)	1.0(1)
O(2)	4e	0	0	0.1622(7)	1.21(13)	1.0(1)

Table 3
Refined atomic positions for $Sr_{10}(CrO_4)_6F_2$

S.G.	$P6_3/m$	$a = 9.9570(1)$ Å	$c = 7.4292(1)$ Å	$R_{wp} = 7.1\%$	$R_{Bragg} = 3.3\%$
Site	x	y	z	B_{eq}	Occ.
Sr(1)	1/3	2/3	−0.0006(5)	0.78(7)	1.0(1)
Sr(2)	0.2502(3)	0.0105(3)	1/4	0.79(5)	1.0(1)
Cr	0.3678(5)	0.3972(6)	1/4	0.63(9)	1.0(1)
O(1)	0.4811(4)	0.3131(4)	1/4	1.01(7)	1.0(1)
O(2)	0.4698(4)	0.5971(4)	1/4	1.24(7)	1.0(1)
O(3)	0.2512(3)	0.3428(3)	0.0683(3)	1.35(6)	1.0(1)
F	0.00000	0.00000	1/4	1.65(8)	1.0(1)

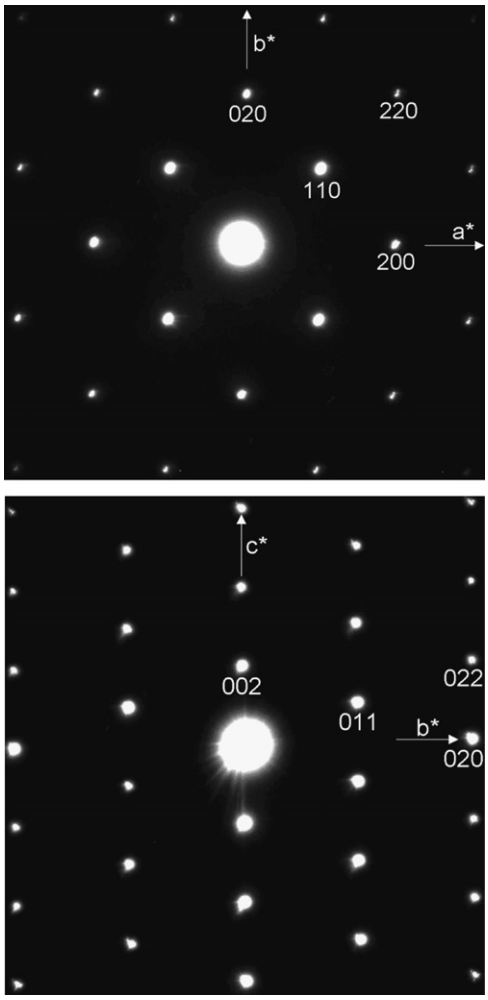

Fig. 3. SAED pattern of Sr_2CrO_4 [0 0 1] (top) [1 0 0] (bottom). Unit-cell parameters $a \approx 3.8$ Å and $b \approx 3.8$ Å, $c = 12.7$ Å with reflection conditions $hk0$: $h+k = 2n$ (top) and $0kl$: $k+l = 2n$.

from the high-pressure synthesis of Sr_2CrO_4, are, however, slightly larger than the previously reported values of $a = b = 3.82$ Å and $c = 12.4$ Å (estimated standard deviations were not reported) [10] (Table 3).

TEM was used to seek evidence of super-structures and/or stacking faults in Sr_2CrO_4. The SAED patterns for the [1 0 0] and [0 0 1] zone axes could be indexed in a tetragonal cell with unit-cell parameters $a = b \approx 3.8$ Å and $c \approx 12.7$ Å

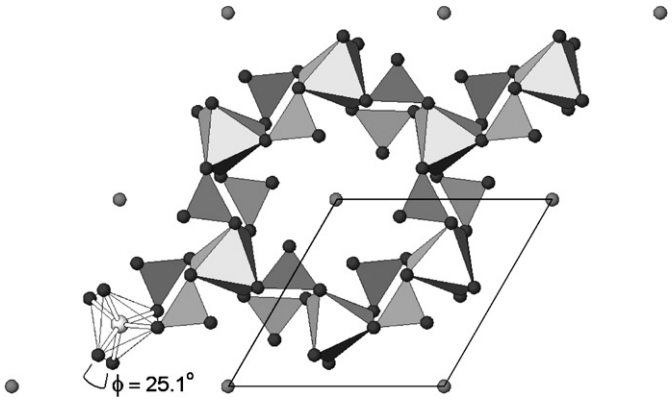

Fig. 4. Structural representation of the apatite $Sr_{10}(CrO_4)_6F_2$. Larger spheres F atoms with SrO_6 octahedra and CrO_4 tetrahedra with O atoms shown as smaller spheres. The unit-cell is indicated by black lines.

(Fig. 3). The conditions limiting the reflections correspond to a body centred lattice (I) $hk0$: $h+k = 2n$ with no other conditions and is consistent with the space group $I4/mmm$. SAED patterns never contained weak reflections indicative of a super-structure, or diffuse intensity suggesting the presence of RP phase intergrowths as observed previously in cuprates [24], titanates [25] and manganates [26] (Fig. 4).

4.2. $Sr_{10}(CrO_4)_6F_2$

Using identical molar ratios of $SrCO_3$, Cr_2O_3 and SrF_2 as for the preparation of Sr_2CrO_4 and the same reaction temperature of 1000 °C with a dwell time of 20 h but applying a slower heating rate of 100 °C h^{-1} to the reaction temperature, resulted in a PXRD pattern typical of an apatite-type compound. It is unclear why modification of the heating rate by just three times resulted in different reaction products; however, one possible explanation is the faster heating rate results in the partial loss of fluorine or fluorine-containing volatile. Because PXRD can be problematic when deriving the atomic positions for elements with low atomic mass e.g. O and F within apatite-type structures [27], neutron diffraction data were collected. This diffraction data was successfully refined using $Ca_{10}(PO_4)_6F_2$ [28] as a structural model with appropriate chemical substitutions (Fig. 5, Table 4). The reliability factors obtained from the refinement indicated that $Sr_{10}(CrO_4)_6F_2$ adopts the

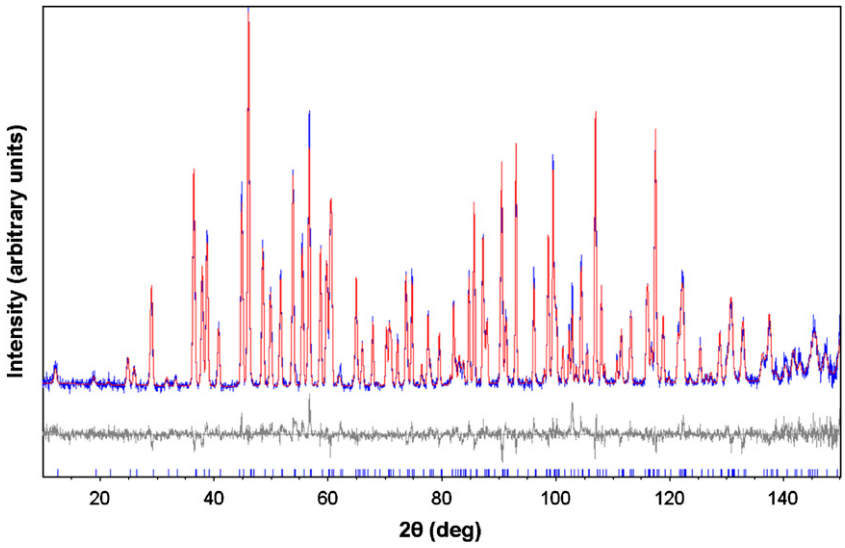

Fig. 5. Rietveld analysis of the PND pattern of $Sr_{10}(CrO_4)_6F_2$.

Table 4
Selected bond lengths (a) and tetrahedron angles (b) for $Sr_{10}(CrO_4)_6F_2$

	Distance (Å)
(a) *Bond*	
Sr(1)–O(1)	2.552(3)
Sr(1)–O(2)	2.595(3)
Sr(1)–O(3)	2.949(3)
Sr(2)–O(1)	2.727(4)
Sr(2)–O(2)	2.506(5)
Sr(2)–O(3)	2.644(4)
Cr–O(1)	1.709(7)
Cr–O(2)	1.724(6)
Cr–O(3)	1.683(4)
Sr(2)–F	2.441(5)
(b) *Angle*	
O(1)–Cr–O(3)	111.1(3)
O(1)–Cr–O(2)	114.4(2)
O(3)–Cr–O(3)	106.6(3)
O(3)–Cr–O(2)	106.6(3)

Table 5
Metaprism twist angle for selected strontium apatites

Chemical formula	Average radius	Metaprism twist angle (°)
$Sr_{10}(PO_4)_6F_2$	1.180	24.3
$Sr_{10}(PO_4)_6(OH)_2$	1.183	23.0
$Sr_{10}(PO_4)_6Cl_2$	1.203	21.1
$Sr_{10}(PO_4)_6Br_2$	1.210	19.6
$Sr_{10}(CrO_4)_6F_2$	1.205	25.1
$Sr_{10}(CrO_4)_6(OH)_2$	1.208	24.8[b]
$Sr_{10}(CrO_4)_6Cl_2$[a]	1.228	22.8
$Sr_{10}(CrO_4)_6Br_2$	1.235	22.1[b]

[a]Reported in the hexagonal space group $P6_3$.
[b]Predicted metaprism twist angle from extrapolation of plot in Fig. 6.

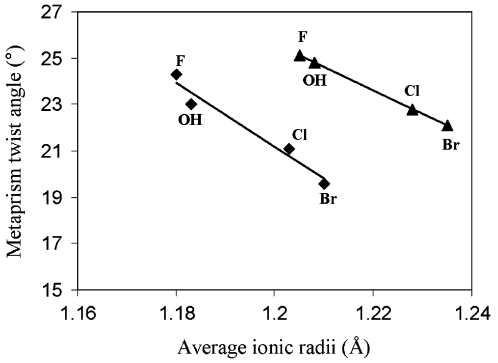

Fig. 6. Plot of metaprism twist angle for strontium phosphate (diamonds) and chromate (triangles) apatites from Table 5.

prototypical hexagonal $P6_3/m$ apatite structure. The CrO_4 tetrahedral bond lengths and angles were quite distorted, as expected for Cr^{5+} which is a d^1 Jahn–Teller ion.

A diagnostic tool known as the metaprism twist angle has been developed to check that refined apatite structures are crystallographically realistic, as the degree of twist is related to the relative sizes of the A, B and X ions [29]. In addition, this approach has been shown to be a sensitive probe for the detection of unexpected departures from ideal stoichiometry or thermodynamic equilibrium. The metaprism twist angle (φ) is defined as the (0 0 1) projected angle of the O(1)–A(1)–O(2) (see Fig. 4), with a compilation of values for available strontium apatites given in Table 5 and Fig. 6. It is evident that as the average ionic radii increases i.e. the size of the tunnel ion increases through the series F > OH > Cl > Br the metaprisms untwist to accommodate the larger anion. Only two examples of strontium chromate apatites have been reported in the literature and based on the near linear relationship shown for the strontium phosphate apatites we predict the metaprism twist angles for the apatites $Sr_{10}(CrO_4)_6(OH)_2$ and $Sr_{10}(CrO_4)_6Br_2$ will be close to 24.8° and 22.1° (see Table 5).

4.3. Magnetic properties

The magnetic and inverse magnetic susceptibility data for Sr_2CrO_4 are quite noisy probably due to the small magnetic moments of the sample and the presence of secondary phase/s (Figs. 7 and 8). The magnetic data do not show any evidence of a transition to long-range magnetic ordering. A Curie–Weiss fitting to the high-temperature $1/\chi$ versus T data was performed; however, it is acknowledged that the numerical values from this fitting should be treated with some caution due to the associated noise and the fact the sample is not single-phase. Nevertheless, the negative Weiss constant, $\theta = -376\,K$, suggests antiferromagnetic interactions are taking place and the calculated effective magnetic moment of $3.12\,\mu_B$ is higher than the calculated spin-only value of $2.83\,\mu_B$ for a d^2 ion with $S = 1$. The origin of this difference points towards a chromium oxidation state different from Cr^{4+}. The antiferromagnetic interactions are in corroboration with the insulating ground state found in a thin film sample of a K_2NiF_4-type Sr_2CrO_4 described by Matsuno et al. [11].

Perovskite and RP phases containing d^2 ($S = 1$) ions are rare and few examples are reported in the literature. Of the known perovskite examples, $AMoO_3$ (A = Ca, Sr and Ba) and $SrCrO_3$ are metallic and Pauli paramagnetic, whereas $CaCrO_3$, $PbCrO_3$, $LaVO_3$ and YVO_3 are semi-conducting and antiferromagnetic [13]. The only reported d^2 ($S = 1$) RP phase is Sr_2MoO_4, which also did not show any long-range magnetic ordering, however this phase was found to display Pauli-paramagnetism and metallic-type behaviour [30].

The magnetic and inverse magnetic susceptibility plots for $Sr_{10}(CrO_4)_6F_2$ yield a linear relationship between $1/\chi$ versus T typical of paramagnetic behaviour (Figs. 9 and 10). A Curie–Weiss fit to the data gives an effective magnetic moment of $1.63\,\mu_B$ per Cr, which is in good agreement with the calculated spin-only value of $1.73\,\mu_B$ for a d^1 ion with $S = \frac{1}{2}$. Only the low temperature part of the curve was used to fit the data in order to avoid the non-linearity due to the small signal for temperature beyond ~200 K.

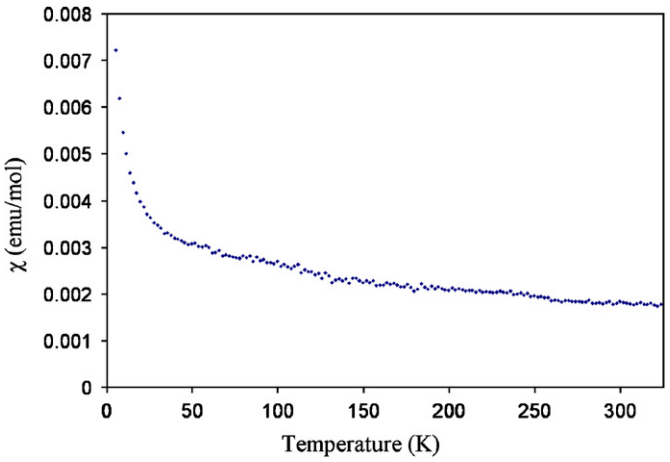

Fig. 7. Magnetic susceptibility versus temperature plot for Sr_2CrO_4 in a magnetic field of 3000 Oe.

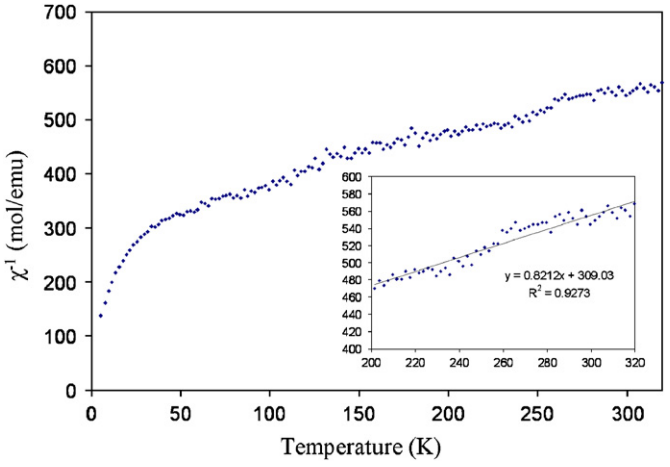

Fig. 8. Inverse magnetic susceptibility versus temperature plot for Sr_2CrO_4 in a magnetic field of 3000 Oe. Inset: Curie–Weiss fit to the linear paramagnetic region.

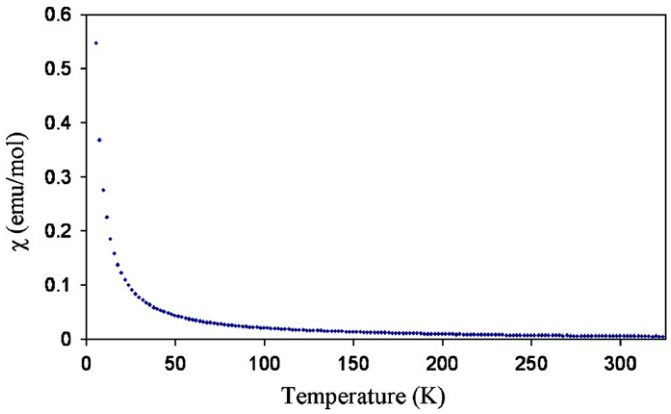

Fig. 9. Magnetic susceptibility versus temperature plot for $Sr_{10}(CrO_4)_6F_2$ in a magnetic field of 3000 Oe.

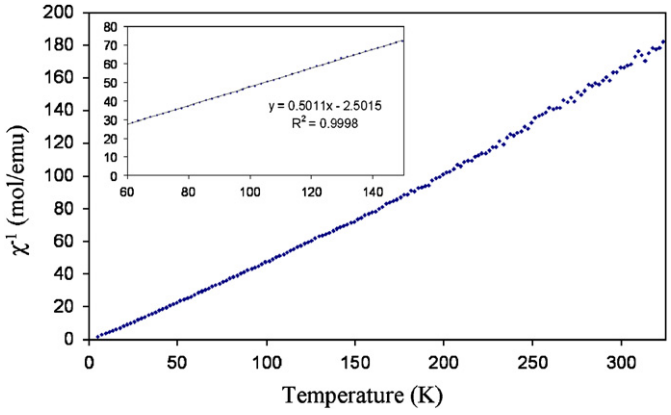

Fig. 10. Inverse magnetic susceptibility versus temperature plot for $Sr_{10}(CrO_4)_6F_2$ in a field of 3000 Oe. Insert: Curie–Weiss fit to the linear paramagnetic region.

4.4. Chemical state of chromium

High resolution XPS spectra of Cr for Sr_2CrO_4 and $Sr_{10}(CrO_4)_6F_2$ are shown in Figs. 11a and b, respectively. For Sr_2CrO_4, deconvolution resulted in two Cr 2p doublets, one at binding energies 576.2, 585.8 eV attributed to Cr^{3+} and the other at 579.7, 588.9 eV associated with Cr^{5+} species (Fig. 11a) which is consistent with earlier reports [21,31–33]. Quantification of the respective peak area revealed the presence of 67 at% Cr^{3+} and 33 at% Cr^{5+}. Assuming the ratio of the two chromium species observed on the surface of the sample is representative of the bulk, this gives approximately $2\frac{1}{3}$ unpaired electrons per unit formula, which in turn yields a calculated spin only value of 3.17 μ_B in good agreement with the observed magnetic moment of 3.12 μ_B. In addition, the mixed Cr^{5+}/Cr^{3+} oxidation states could explain why although the site refined to full occupancy for Cr^{4+} a quite high thermal parameter was also observed as noted earlier. However, as this sample is not single phase and the absolute values obtained for the quantities of Cr^{5+} and Cr^{3+} should be treated with caution. In addition, it is possible that some of the Cr^{5+} present in the sample is reduced to Cr^{3+} in the XPS chamber [31].

It is unknown whether the chromium oxidation states found in this work for Sr_2CrO_4 are different from that prepared in previous work using high-pressure methods [10] as no XPS or magnetic measurements were carried out. However, the mixed Cr^{5+}/Cr^{3+} in the sample prepared in this work may explain why the refined lattice parameters for Sr_2CrO_4 prepared at ambient pressure are dilated compared to than those obtained in the high-pressure synthesis as the ionic radii of Cr^{3+} (0.62 Å) is large compared to Cr^{4+} (0.55 Å) [34].

The Cr 2p XPS of $Sr_{10}(CrO_4)_6F_2$ (Fig. 11b) also showed two doublet peaks at binding energies of 579.3, 588.5 eV and 577.2, 585.9 eV, consistent with Cr^{5+} and Cr^{3+}, respectively [21,31–33]. From the relative peak area it is seen that the concentration of Cr^{5+} species is higher on the surface as compared to Cr^{3+}, and as the magnetic studies indicate pure Cr^{5+}, the calculated effective magnetic moment cannot be reconciled with the presence of Cr^{3+}

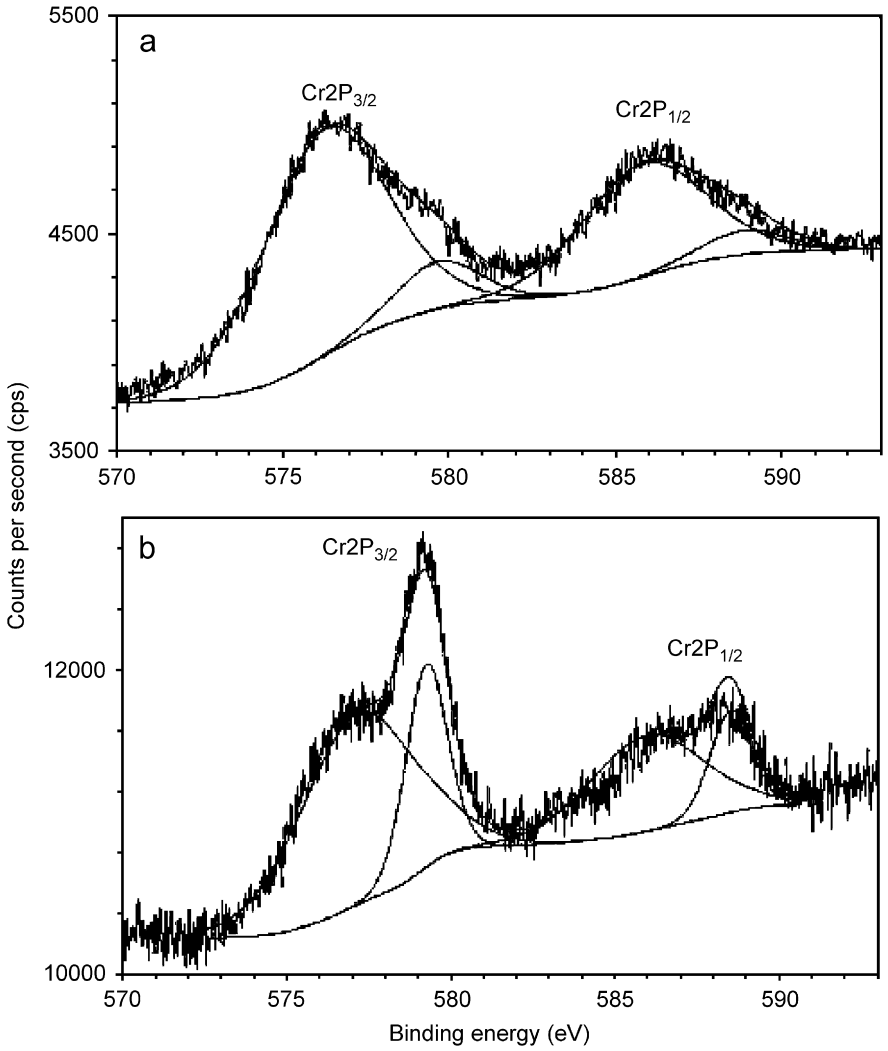

Fig. 11. X-ray photoelectron curve fitted spectrum of Cr 2p in: (a) Sr_2CrO_4; (b) $Sr_{10}(CrO_4)_6F_2$.

with three unpaired electrons. This anomaly arises due to the in situ reduction of Cr^{5+} under X-ray irradiation [31] and the apatite contains Cr^{5+} primarily in the bulk, corroborating with the magnetic measurement. In addition, it was observed that the relative amount of Cr^{3+} increased when the sample was argon ion etched within the XPS chamber.

Fig. 12 shows the high resolution O 1s spectrum of Sr_2CrO_4 and $Sr_{10}(CrO_4)_6F_2$ samples. The O 1s peak of Sr_2CrO_4 comprised of main component peak at 530.6 eV, which is attributed to lattice oxygen and a minor component peak at ~535 eV due to chemisorbed water species (which are typically present even under ultra-high vacuum conditions) as noted in earlier reports [35]. The broad O 1s peak of $Sr_{10}(CrO_4)_6F_2$ can be deconvoluted into two component peaks at 530.0 and 531.8 eV. The former is due to lattice oxygen and the latter can be due to apatitic oxygen (CrO_4^{3-} similar to PO_4^{3-}) or adsorbed OH^- or CO_3^{2-} species [36]. An additional peak at higher BE (~534.8 eV) is due to adsorbed water on the sample surface.

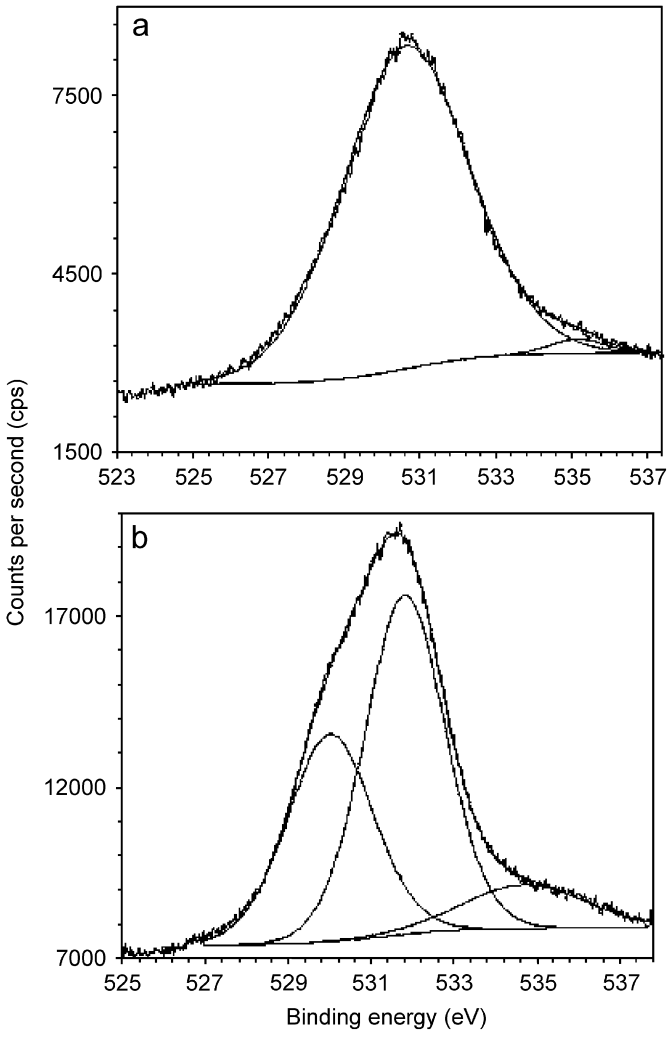

Fig. 12. X-ray photoelectron curve fitted spectrum of O 1s in: (a) Sr_2CrO_4; (b) $Sr_{10}(CrO_4)_6F_2$.

5. Conclusions

The K_2NiF_4-type phase Sr_2CrO_4 was prepared at ambient pressure for the first time and characterised using a combination of SAED and PXRD. The material displays antiferromagnetic interactions but no transition to long-range magnetic ordering. The structure of $Sr_{10}(CrO_4)_6F_2$ has been refined using powder neutron diffraction for the first time and both materials provide rare examples of materials containing chromium in the +5 oxidation state. The presence of pentavalent chromium was unequivocally assigned using a combination of XPS and magnetic susceptibility measurements.

Acknowledgments

This work was supported through a joint NRC-A*STAR research program on "Advanced Ceramic Methods for the Co-stabilisation and Recycling of Incinerator Fly Ash with Industrial Wastes". The authors would like to thank Dr. Wim Klooster for collecting the neutron diffraction data.

References

[1] J.G. Bednorz, K.A. Müller, Z. Phys. B Condens. Matter. 64 (1986) 189.
[2] M.T. Weller, C.S. Knee, J. Mater. Chem. 11 (2001) 701.
[3] S.A. Wolf, D.D. Awschalom, R.A. Buhrman, J.M. Daughton, S. von Molnár, M.L. Roukes, A.Y. Chtchelkanova, D.M. Treger, Science 294 (2001) 1488.
[4] S.N. Ruddlesden, P. Popper, Acta Cryst. 10 (1957) 538; S.N. Ruddledsen, P. Popper, Acta Cryst. 11 (1958) 54.
[5] K. Yamaura, D.P. Young, R.J. Cava, Phys. Rev. B 63 (2001) 064401.
[6] Y. Moritomo, A. Asamitsu, H. Kuwahara, Y. Tokura, Nature 380 (1996) 141.
[7] D. Balz, K. Plieth, Z. Elektrochem. 59 (1955) 545.
[8] K.A. Wilhelmi, Ark. Kemi. 26 (1967) 157.
[9] B. L Chamberland, M.P. Herrero-Fernandez, T.A. Hewston, J. Solid State Chem. 59 (1985) 111.
[10] J.A. Kafalas, J.M. Longo, J. Solid State Chem. 4 (1972) 55.
[11] J. Matsuno, Y. Okimoto, M. Kawasaki, Y. Tokura, Phys. Rev. Lett. 95 (2005) 176404.
[12] B.L. Chamberland, Solid State Comm. 5 (1967) 663.
[13] C.N.R. Rao, Annu. Rev. Phys. Chem. 40 (1989) 291.
[14] D. Pelloquin, A. Wahl, A.C. Masset, A. Maignan, C. Michel, B. Raveau, J. Solid State Chem. 154 (2000) 375.
[15] C. Martin, A. Maignan, M. Huvé, M. Hervieu, C. Michel, B. Raveau, Physica C 179 (1991) 1.
[16] K.A. Wilhelmi, O. Johnson, Acta Chem. Scand. 19 (1965) 177.
[17] E. Banks, K.L. Jaunarajs, J. Inorg. Chem. 4 (1965) 78.
[18] E. Herdtweck, Acta Cryst. C 47 (1991) 1711.
[19] H.M. Rietveld, Acta Crystallogr. 22 (1967) 151; H.M. Rietveld, J. Appl. Crystallogr. 2 (1969) 65.
[20] R.W. Cheary, A. Coelho, J. Appl. Cryst. 25 (1992) 109.
[21] C.D. Wagner, W.M. Riggs, L.E. Davis, J.F. Moulder, G.E. Muilenberg, Handbook of X-ray photoelectron spectroscopy, Perkin–Elmer Corporation, Physical Electronics Division, 1979.
[22] N. Fairley, A. Carrick, The Casa Cookbook, Part I, Acolyte Science, 2005.
[23] W.V. Rochat, J.N. Gerlach, G.L. Gard, Inorg. Chem. 9 (1970) 998.

[24] M. Hervieu, C. Michel, B. Raveau, J. Less Common Met. 150 (1989) 59.
[25] K.D. Hawkins, T.J. White, Philos. Trans. R. Soc. 336 (1991) 541.
[26] J. Sloan, P.D. Battle, M.A. Green, M.J. Rosseinsky, J.F. Vente, J. Solid State Chem. 138 (1998) 135.
[27] P.H.J. Mercier, Y. Le Page, P.S. Whitfield, L.D. Mitchell, J. Appl. Cryst. 39 (2006) 369.
[28] K. Sudarsanan, P.E. Mackie, R.A. Young, Mater. Res. Bull. 7 (1972) 1331.
[29] T.J. White, C. Ferraris, J. Kim, S. Madhavi, Rev. Miner. Geochem. 57 (2005) 307.
[30] N. Shirakawa, S.I. Ikeda, Physica C 364–365 (2001) 309.
[31] D. Gazzoli, M. Occhiuzzi, A. Cimino, G. Minelli, M. Valigi, Surf. Interface Anal. 18 (1992) 315.
[32] L. Giraldo, C. Pfaff, C.M. Lopez, F. Machado, B. Mendez, J. Goldwasser, M.M.R. De Agudelo, S. Rondon, M. Houalla, D.M. Hercules, Surf. Interface Anal. 24 (1996) 863.
[33] Y. Aoki, H. Kano, J. Solid State Chem. 156 (2001) 370.
[34] R.D. Shannon, Acta Crystallogr. 32 (1976) 751.
[35] M.C. Biesinger, C. Brown, J.R. Mycroft, R.D. Davidson, N.S. McIntrye, Surf. Interface Anal. 36 (2004) 1550.
[36] S. Kaciulis, G. Mattogno, L. Pandolfi, M. Cavalli, C. Gnappi, A. Montenero, Appl. Surf. Sci. 151 (1999) 1.